Using a structural approach to identify relationships between soil and erosion in a semi-humid forested area, South India

Laurent Barbiero, H.R. Parate, Marc Descloitres, Adelphe Bost, S. Furian, M.S.M. Kumar, C. Kumar, J.J. Braun

Using a structural approach to identify relationships between soil and erosion in a semi-humid forested area, South India

Laurent Barbiéro[a,b,*], Harshad R. Parate[b], Marc Descloitres[c,b], Adelphe Bost[b], Sônia Furian[d,b], M.S. Mohan Kumar[b], C. Kumar[b], Jean-Jacques Braun[a,b]

[a] *IRD, LMTG-OMP, UMR 5563, Laboratoire des Mécanismes de Transfert en Géologie, 14 Av. E. Belin, F-31400 Toulouse, France.*

[b] *Indo-French Cell for Water Sciences (IRD-IISc Joint Laboratory), Indian Institute of Science, 560 012, Bangalore, India.*

[c] *IRD, UR012-LTHE, UMR/CNRS-IRD-INPG-UJF, B.P. 53, 38041 Grenoble Cedex 9, France.*

[d] *Dep. Geografia, Avenida Prof. Lineu Prestes, 338, CEP 05508-000, Universidade de São Paulo-SP, Brasil.*

* Corresponding author.

E-mail address: barbiero@civil.iisc.ernet.in

Abstract

Biogeochemical and hydrological cycles are currently studied on a small experimental forested watershed (4.5 km²) in the semi-humid South India. This paper presents one of the first data referring to the distribution and dynamics of a widespread red soil (Ferralsols and Chromic Luvisols) and black soil (Vertisols and Vertic intergrades) cover, and its possible relationship with the recent development of the erosion process. The soil map was established from the observation of isolated soil profiles and toposequences, and surveys of soil electromagnetic conductivity (EM31, Geonics

Ltd), lithology and vegetation. The distribution of the different parts of the soil cover in relation to each other was used to establish the dynamics and chronological order of formation. Results indicate that both topography and lithology (gneiss and amphibolite) have influenced the distribution of the soils. At the downslope, the following parts of the soil covers were distinguished: i) red soil system, ii) black soil system, iii) bleached horizon at the top of the black soil and iv) bleached sandy saprolite at the base of the black soil. The red soil is currently transforming into black soil and the transformation front is moving upslope. In the bottom part of the slope, the chronology appears to be the following: black soil > bleached horizon at the top of the black soil > streambed > bleached horizon below the black soil. It appears that the development of the drainage network is a recent process, which was guided by the presence of thin black soil with a vertic horizon less than 2 m deep. Three distinctive types of erosional landforms have been identified:

1. rotational slips (Type 1);
2. a seepage erosion (Type 2) at the top of the black soil profile;

Types 1 and 2 erosion are mainly occurring downslope and are always located at the intersection between the streambed and the red soil-black soil contact. Neutron probe monitoring, along an area vulnerable to erosion types 1 and 2, indicates that rotational slips are caused by a temporary water table at the base of the black soil and within the sandy bleached saprolite, which behaves as a plane of weakness. The watertable is induced by the ephemeral watercourse. Erosion type 2 is caused by seepage of a perched watertable, which occurs after swelling and closing of the cracks of the vertic clay horizon and within a light textured and bleached horizon at the top of black soil.

3. a combination of earthflow and sliding in the non-cohesive saprolite of the gneiss occurs at midslope (Type 3). Type 3 erosion is not related to the red soil-black soil system but is caused by the seasonal seepage of saturated throughflow in the sandy saprolite of the gneiss occurring at midslope.

Keywords: Erosion, Structural Analysis, Electromagnetic Induction, Chromic Luvisol, Vertisol, South India.

1. Introduction

In recent years, several studies are carried out to understand the bio-geochemical cycles of major and trace elements, to calculate the mechanical erosion and chemical weathering rates, to estimate the role of the major parameters (relief, climate, lithology, vegetation, anthropisation…) that are likely to control the chemical weathering processes, to quantify the effects of rock chemical weathering on the carbon cycle and to find its potential role on climate changes (Gaillardet et al., 1997; 1999; Oliva et al., 2003). The integrated study of small watersheds is one of the best way to provide direct and accurate information for the analysis of ecosystems. Although this integrated ecosystem approach is common for the temperate zone, it has not yet been widely applied to the tropics and especially under semi-humid climate (White et al., 1998, Braun et al., 2005). Such a study is currently developed on small experimental watersheds in South India, namely, surface and groundwater flow (Descloitres et al., 2007), regolith thickness and chemical weathering, physical erosion, dynamic of the soil cover and including interactions among the aforementioned aspects (Braun et al., 2006). Although it is today widely known that internal transformation of a soil cover can influence or even govern landscape evolution through intensification or decrease of physical erosion (whatever could be the parental material or topographical gradient, Boulet et al., 1977; Planchon et al., 1987; Filizola and Boulet, 1996; Barbiéro et al., 1998; Furian et al., 1999), the soil cover itself is still a black box in many studies on soil erosion. Moreover, very little is known about natural erosion in forested areas in South India where human activity is minimal, although features of erosion have been observed. The aim of this study is to identify the dynamic and to present the main factors intrinsic to the soil cover that govern natural erosion on a forest area with a widespread red and black soil system, by using a structural and a spatially distributed approach.

2. Site

In South India, the Western Ghats parallel to the western coast of the peninsula form an orographic barrier, inducing an important climatic gradient, with annual rainfall decreasing progressively from about 5000 mm in the west, to less than 750 mm just 80 km to the east (Pascal, 1982; Fig. 1). The climatic sequence (climosequence) is associated with changes in landscape geomorphology from convex hills intermittent with flat floors to long concave glacis (Gunnell and Bourgeon, 1997; Gunnell, 2000). In connection with the geomorphological changes, the soil types (FAO-ISRIC-ISSS, 1998) range from Ferralsols to thin red soils (Chromic Luvisols) associated with black soils (Vertisol, Vertic intergrades) in the climatic semi-humid transition area, and in the semi-arid area we find Calcic Luvisol and Calcic Vertisol (Murthy et al., 1982; Pal and Despande, 1987; Bourgeon, 1991; Jacks and Sharma, 1995, Gunnell, 2000). This association of red soils (Luvisols) and black soil (Vertisols) is widespread on the semi-humid to semiarid area of the Deccan plateau (Bourgeon, 1991). The passage in the clay mineralogy from the kaolinite-dominated humid area to the smectite-dominated semi arid area is achieved progressively via an intermediate area with 2:1 K clay such as illite and sericite (Bourgeon and Pedro, 1992).

Red soils occurring in the current seasonal semihumid to semiarid conditions (<1500 mm annual rainfall and high evapotranspiration) have been considered as Paleosols or relict soils (non buried Paleosols) that formed in an earlier period with a moister climate than the present, but this assertion is still under debate. Some authors consider that the climatic conditions are not conducive to the soil-forming processes of red soils such as deep weathering and kaolinite formation (Bronger and Bruhn, 1989; Brückner and Bruhn 1992). However, Gunnell and Bourgeon (1997) emphasize that the presence of clay minerals yielding an X-Ray diffraction peak at 7 Å in dry climatic zone does not necessarily mean that these are inherited from a Paleosol formed in more humid periods in the past.

They suggested further analysis, and in particular the comprehensive down-profile consideration of the entire spectrum of minerals, before reaching a conclusion. In the prevailing semiarid conditions (<900 mm annual rainfall), secondary carbonate is currently accumulating in the saprolite and lower parts of the red soil horizons (Bronger et al., 2000). Micromorphological studies of the calcrete in the semiarid area reveal a multistage origin (Durand et al., 2006a) and recent dating of calcrete nodules suggests fairly stable climatic conditions at the ≥ 200 ky time scale (Durand et al., 2006b).

The climatic and pedoclimatic conditions are decisive in the formation of red soils (Bourgeon, 1991), whereas the formation of black soils depends mainly on the slow down of the solution and lack of drainage usually in bottom part of the landscape. In Black soils, the presence of smectite clay minerals causes appreciable shrink–swell, which induces formation of cracks and distinctive structural elements such as wedge-shaped peds with smooth or slickensided surfaces (Bourgeon, 1991).

Field work was carried out on a 4.5 km^2 watershed located in Bandipur National Park, close to the Mulehole check post at 11º 44' N and 76º 27' E (Karnataka state, Chamrajnagar district). The watershed area is mostly undulating with gentle slopes and the elevation of the watershed ranges from 820 to 910 m above sea level. Because it belonged to the hunting reserve of the Maharaja of Mysore, the region has been preserved from agricultural activity at least since the 17th century. Later it was incorporated into the Bandipur National Park, and today the only human activities are limited to surveillance by the rangers of the Forest Department.

The studied site is located in the climatic semi-humid transition area (Fig. 1) and the mean annual rainfall (n = 20 years) is 1120 mm. The climate is characterized by recurrent but non-periodic droughts, depending on monsoon flows. The mean yearly temperature is around 27ºC. Streams are temporary, flowing for a few hours to a few days after the stormy events of the rainy season. Rainfall and runoff measured at the outlet of the Mulehole watershed were respectively 431 mm and 1 mm in 2003, 1216 mm and 59 mm in 2004, and 1434 mm and 181 mm in 2005.

The substratum belongs stratigraphically to the Precambrian Dharwar supergroup (Moyen et al., 2001) and consists of gneiss with amphibolites and quartz dykes. The mean strike value is N80°, with a dip angle ranging from 75° to the vertical. The vegetation consists of dry deciduous forest (Pascal, 1982, 1986; Agarwala, 1985) where 4 different types of vegetation have been identified: 1 - a forest with vegetation mainly dominated by three species, namely *Anogeissus latifolia, Terminalia alata* and *Tectona grandis,* called 'ATT facies'. 2 - a vegetation called 'Shorea facies' characterized by the presence of *Shorea roburghii* and *Lagerstroemia microcarpa.* 3 - the 'Swamp facies' consisting of grass-covered glades with scattered trees (*Ceristoides turgida*). 4 – the discontinuous 'riverine facies' along the talwegs characterized by the presence of *Syzygium cumini, Mangifera indica, Ficus recemosa* and *Derris indica*. The first 3 above-mentioned vegetation 'facies' have been identified in the Mulehole watershed, whereas the fourth one was not clearly developed and/or occupied very small area.

3. Method

3.1. Study at the watershed scale

A contour Digital Elevation Model (DEM) was generated from 2780 topographical measurements on the area (Fig. 2), with higher density close to the talwegs and to the main topographical changes. An exhaustive GPS georeferenced survey of the streambeds and the soil erosion pattern was carried out for the entire watershed. The eroded soil volume was roughly estimated by measuring the length, width and thickness of each eroded area in relation to the surrounding non-eroded area.

Electromagnetic induction is becoming widespread for soil survey in general, although it has been used mainly for the monitoring of spatial and temporal changes in soil salinity (Corwin et al., 2005). Preliminary studies on the watershed have shown that red and black soils have a different apparent

electrical conductivity (EC). Therefore, soil distribution was first attempted by conducting an electromagnetic conductivity survey, using an EM31 portable device (Geonics Ltd, Ontario, Canada). The device measures an apparent conductivity (EC_m values) in milliSiemens per metre (mS/m). The EM31 has a fixed 3.66 m space between the coils (transmitter and receiver) and the measurements were carried in the vertical dipole configuration, which affords an investigation depth of about 4 to 6 m (McNeill, 1980). The measurements were carried out along 31 North-South oriented transects and with a space of 100 meters between the transects (Fig. 2). The measurement points were taken and stored automatically by a data logger every 5 seconds. A Global Positioning System (GPS) was coupled with the EM31 device in order to get the geographical coordinates of each measurement point (Cannon et al., 1994). The survey was carried out in January 2004, i.e. in the middle of the dry season.

The EC_m data underwent a geostatistical treatment before kriging. Duplicates were removed from the data set before treatment, on the basis of a 2 m tolerance in the X and Y directions. These duplicates are due to local difficulties in progressing through the vegetation or in crossing obstacles (topographic accidents) during the survey. A chi-squared test showed that the data might not be assumed to have a normal distribution. Therefore, the calculation was performed on a theoretical distribution of the data by lognormal transformation as recommended by Dowd (1982),

$$z(x_i)=\ln(s(x_i)) \quad (1)$$

where $s(x_i)$ is the EC_m data at x_i, $z(x_i)$ is the log-transformed data. An estimate of the samples variogram is given by the formula:

$$\gamma(h) = \frac{1}{2N(h)} \sum_{i=1}^{N(h)} (z(x_i) - z(x_i + h))^2 \quad (2)$$

Where N(h) is the number of pairs of points and $z(x_i)$ and $z(x_{i+h})$ are the logarithms of the EC_m values at x_i and x_{i+h}. Raw and directional variogram were calculated to detect a possible anisotropy in the field. The kriged map is built from a model of variogram fitted to the sample variogram.

In order to relate the EC_m map to the soil distribution, forward modelling was carried out using the PCloop software (Geonics, Ltd) and was based on (i) the theoretical response of the EM31 over an horizontally layered medium (McNeill, 1980); (ii) resistivity measurements of representative horizons in red and black soils along soil profile; and (iii) resistivity logging down auger holes drilled into representative soils (Ferralsols, Luvisols and Vertisols).

A geological survey was carried out from the identification of about 300 georeferenced rock outcrops within the watershed and the extrapolation of the data was carried out using the EC_m survey.

The development of vegetation depends narrowly on the hydric regime of the soil, and consequently on the type and thickness of soil. Therefore, a survey of the three main types of vegetation, namely the ATT, Shorea and Swamp facies was carried out across the watershed in order to extrapolate the soil data.

3.2. Comprehensive study along soil sequences

Two soil sequences were studied on the watershed (Fig. 2). An existing spoon-shaped erosional landform (rotational slip type) was targeted for the excavation of a 80 m long trench (T1) in order to understand the soil morphology of the portions of landscape vulnerable to soil erosion (Fig. 3, Fig. 4a). The second soil sequence (T2) located where the streambed appears to be currently incising (just a few meters upstream from the current incision, Fig. 4e), was studied in order to understand if any specific morphology of the soil cover could favour the development of the talweg.

The soil pattern was studied in detail, emphasizing the geometrical relationships between the different horizons identified from basic field observations (colour, texture, structure, porosity,

presence of coarse elements, intensity of biological activity…). The procedure follows routine techniques developed by Boulet et al. (1982) and Fritsch et al. (1992).

In the first step, 2D electrical imaging was performed around toposequence T1 to locate the red soil / black soil contact and to characterise its morphology. Five boreholes were drilled down to the saprolite in the red soil, black soil and transition area, along a line parallel located at a distance of 5 m from T1 (Fig. 3). The different horizons of the boreholes were identified and compared to the description from the trench T1 in order to map the layout of the red soil – black soil system. Soil moisture was monitored during the rainy seasons 2004 and 2005 through neutron probe measurements (soil moisture probe type I.H. II, Didcot Instrument Co. Ltd., Abingdon Oxon, England). Measurements were carried out at every 10 cm, every 15 days, and daily during heavy rainy periods. Between two successive neutron probe measurement periods, the boreholes were clogged with inflatable rubber tubes inserted into the holes in order to prevent any infiltration from the topsoil runoff or along the hole during rainfall.

For each horizon, a relationship was established between the neutron probe measurements and the volumetric water content. For this purpose, bulk samples were collected while drilling holes and immediately placed and sealed in metallic boxes. Simultaneously the neutron probe measurements were carried out at the corresponding depth. Gravimetric water content was determined in the laboratory by weighing the samples before and after oven drying for 24 hours at 105 °C. This procedure was carried out at the end of the dry season (dry state) in the monitored holes and at the end of the monsoon season (wet state) in new holes drilled at about 50 cm away from the previous ones. The bulk density was measured using the paraffin method on aggregates collected along the trench T1 in each horizon (Singer, 1986). The volumetric water content in the boreholes was estimated by multiplying the gravimetric water content by the bulk density of the corresponding horizon.

The calibration was established for each horizon using linear regression between the volumetric water content against the R/Rw ratio, where R denotes the number of counts per second of neutron

probe in soil and Rw denotes the number of counts per second in a water standard. The calibration was established on a volumetric water content range of 16 to 31% in red soil (horizons 2, 3, 4 and 5), 21 to 35% in black soil (horizons 7, 8, 9, 10 and 11), 12 to 30% in organic topsoil horizon (6), and 13% to 29% in the saprolite (horizons 1 and 13).

4. Results

4.1. EC_m measurements and EC_m survey

From the 10935 EC_m measurement points, 439 duplicates were discarded before treatment. The conductivity values range between 0.1 and 52 mS/m, with an average value of 7.21 mS/m, and a standard deviation of 7.06 mS/m. The variation coefficient (0.98) indicates a low dispersion of the data around this average value.

The experimental variogram built from log-transformed EC_m data is presented in Fig. 5. A slight anisotropy is detected by comparing the raw and directional variogram, showing a higher dependence of the EC_m values in the direction N63.6° (East-Northeast/West-Southwest). This anisotropy was taken into account for the kriging computation. In N63.3° direction the experimental variogram shows a nugget effect of almost zero, a range of about 300 m and the scale of 0.105 (log value), and therefore it fits better with an exponential model with the following characteristics: Scale = 0.105; range = 300 m.

The kriged map presented on Fig. 6 shows that the soil electromagnetic conductivity is not distributed regularly throughout the watershed. High conductivity values are located in the flat bottom part of the watershed and on some areas on the crest line, while low conductivity values are mainly observed along the slopes.

4.2. Geology

As presented on the lithological map (Fig. 7), most of the watershed is developed on paragneiss (peninsular gneiss) and basic rocks (amphibolite and derived facies). The latter cover about 17% of the watershed and are not related to any particular topographic locations. They can be found anywhere, namely in the valley bottom, along the slope or on the crest line. Paragneiss is dominant and consist mainly of quartz, feldspar (plagioclase and potassic) with a low quantity of biotite. Bedrock exposures are usually poorly weathered, except along the talweg at the higher third of the watershed where the gneiss occurs as non-cohesive loose saprolite.

4.3. Vegetation survey and soil-vegetation relationships

The ATT vegetation type is dominant, covering about 70% of the watershed, and has developed on both, thick red soils and thin black soils with a vertic horizon usually less than 1 m thick. A few isolated *Ceristoides* trees have developed into the ATT type although they are usually associated with Swamp vegetation. In this case, the presence of the *Ceristoides* is always associated to higher EC_m values and with the presence of a 0.5-m-thick black soil developed from an alternation of metre-thick veins of gneiss and amphibolite saprolite. However, *Ceristoides* is absent in the southeastern part of the watershed with ATT vegetation type and high EC_m values. Observations carried out along auger holes and a pit indicated that in this area, close to the topsoil (e.g. at 0.3 m depths), we also find the presence of a conductive saprolite consisting of weathered amphibolites.

The Swamp vegetation type is mainly located in the low parts of the watershed with some spots along the crest line, and always associated with higher EC_m values. Field observations indicated that it grows exclusively on thick black soils (>2 m) in the lower part of the watershed as well as on the crest, covering about 5% of the area. The *Shorea* vegetation type covering about 15% of the

watershed occurs on very shallow red soil overlying a sandy gneiss saprolite found very close to the topsoil (0.2-0.4 m below the topographic surface).

4.4. Soil distribution

The map presented on Fig. 8 was drawn from the overlay of EC_m, lithology and vegetation survey and crosschecked with about 60 isolated soil observations. A clear relationship was observed between the soil electromagnetic conductivity and certain soil characteristics explained below. Ferralsols are usually 2 to 3 m thick and have lower conductivity, whereas Luvisols are thinner and have higher conductivity. Since the EM31 response depends on both the thickness and the apparent conductivity, no significant contrast was detected with this method, and it does not make it possible to discriminate the spots of Ferralsols from the surrounding Chromic Luvisols. Therefore, both Ferralsols and Luvisols have been grouped together into a red soil unit. The boundary between red and black soils was identified at an EC_m value of 8-10 mS/m (0.9 to 1 log value) and EC_m values above 18 mS/m (1.26 log value) indicates thick black soil, and this boundary is strictly in agreement with the distribution of the Swamp vegetation type. However, although the relationship between EC_m and soil type was tested in many places on the watershed, it was not valid for the south-eastern part where the saprolite of an amphibolite type rocks was observed close to the topsoil and associated to higher EC_m values (Fig. 7).

The major part of the watershed is covered by red soils that are about 1 or 2 meters thick and can reach about 4 meters at certain locations. Thin red soils (about 0.2 to 0.5 m thick) overlying loose gneiss saprolite and associated with the *Shorea* vegetation are mainly located on the central wash divide between the two main talwegs and in a discontinuous crescent-shaped area along the slopes. Black soils have developed on two types of location: (i) the low-lying area, occupying the lower part of the slope and the flat valley bottoms. Black soil areas are about 2 m thick at the perimeter but can reach more than 6 meters at the centre. They have developed from both gneiss and amphibolite

saprolite. (ii) At higher levels black soils are about 0.2 to 0.5 m thick, except at the depressions (50 to 100 m in diameter) on the crest line where the black soils can reach 2.5 m. They are always associated with gneiss, which alternates with amphibolites.

4.5. Streambed features and soil-streambed relationships

Although the stream is meandering in the valley bottom, there is no undermining of the banks in the convex curves or point-bar deposits inside meanders, and the stream seems to have sunk on its own bed. The bottom of the streambed is steep-sided of about 2 to 4 m and flows on the hard saprolite on the lower 2/3 of the watershed, and on the soil cover on the upper 1/3 part of the watershed. At several places of lower third of the watershed, roots of trees such as *Tectona grandis* are occasionally crossing the streambed at about 1 m from the bottom (Fig. 4g). A peculiar distribution of streambed was observed in relation to the black soil developed downslope: When the streambed enters a black soil area, it does not flow straight through it but gets around the thick black soil area and meanders into the thin black soil as shown on Fig. 8.

4.6. Types and distribution of erosion spots

All the erosion spots are located in the vicinity of the talwegs (i.e. less than 30 meters). Three main types of erosion were identified (Sidle et al., 1985) and their descriptive statistics are given in Table I.

The first and the most widespread type is a rotational slip (25 sites) with vertical edges, whose standard dimensions are about 5 m wide, 25 m long and 2 m deep (Fig. 4a and d). In most of the slips, the material has been subsequently evacuated towards the stream. This type of erosion is well developed in the bottom area and within the lowest third of the watershed. All the slips are distributed at the crossing between the streambeds and the iso-conductivity line of 11 mS/m, i.e. very

close to the contact between red and black soils. More precisely they are slightly inside the black soil area (Fig. 8) and always develop towards the red soil domain.

The second type (14 sites) refers to superficial erosional scars whose widths and lengths are about 2 or 3 meters, respectively, with depths of about 0.5 m thick (Fig. 4b). This landform is provoked by occasional seepage occurring at the top of the black soils at a textural contrast between a clay horizon and the sandy topsoil horizons with many coarse elements such as ferruginous nodules, quartz, etc. It was found in several places such as at the bottom parts of the watershed, along the slopes and close to the crest line.

The third type (7 spots) is much wider than type 1 and 2 and the average eroded soil volume reaches 3300 m^3 per spot (Fig. 4c). Although the lower part is predominantly a flow movement, the upper part involves recurrent small sliding. It has developed in the vicinity of the streambeds, but only at places where the non-cohesive saprolite of the gneiss is close to the topsoil. In other words it occurs within the uppermost third of the watershed and at the intersection between the streambeds and the crescent-shaped area where the *Shorea* vegetation was surveyed.

4.7. Soil morphology at the red soil-black soil contact

Fig. 9a shows the soil distribution pattern along the contact between red and black soil, which can be easily divided into two domains. Upslope, a 3 m-thick red soil overlies white gneiss saprolite. In the saprolite (1) the structure and the sub-vertical foliation of the rock itself is still preserved. Five horizons (2 to 6) have been distinguished in the red soil. From the bottom to the top of the profile, these horizons differs mainly by their colour evolving from grey (7.5YR6/1), brown (7.5YR4/4), reddish-brown (7.5 to 5YR4/4) then red (5YR4/3 to 4/2), and also by the structure evolving from angular blocky to micro-aggregate and granular. Ferruginous nodules (3 to 6 mm) are observed from the top of the gneiss saprolite to the topsoil horizon (6), with a maximum of concentration at the top

of horizon (4). The above-described horizons (2 to 6) are parallel to each other and to the topography of the slope.

Downslope, lateral morphological changes occur from the bottom of the soil to almost close to the topsoil, where clay films coat the structural faces of the soil aggregates. The presence of clay films defines horizon (7), which intersects horizons (2), (3), and (4) without changing their respective structures. The clay films become thicker in horizon (7) while moving downslope and it progressively turns into a 10 to 20 cm-thick clay horizon (8), which is dark red-brown (5 to 7.5YR3/2 to 4/2) with a coarse angular blocky structure. The blocks are compact, hard and separated by vertical and sub-horizontal cracks but without slickensides. Horizons (7) and (8) have many ferruginous nodules, and they extend the maximum of nodules observed into horizon 4. Horizon (9) differs from horizon (8) wherein the colour shifts to dark brown (5 to 7.5YR3/2 to 2/2) and the structure becomes clearly vertic (15 cm wide) with sub-horizontal slickensides. Horizon (10) below (9) is horizontal, concordant with the flat valley bottom occupied by black soil cover on the right side of Fig. 9b. It is more greyish (10YR3/1 to 3/2) and the vertic structure of about 7 to 8 cm is still dominant but with an angular blocky sub-structure. At horizon (11) the soil material progressively turns into saprolite of the gneiss in which the lithologic structure is still preserved. Isolated volumes of the saprolite preserving the orientation of the parental material are observed up to the base of horizon (10).

In addition to the above-mentioned description, two bleached horizons have been identified, discriminated from a contrast in colour (lighter) and texture (more sandy) and structure (massive). The first one (12) lies above horizons (7) and (8), evolving downslope progressively from dark (5YR3/2) clay-sand to light (7.5YR4.5/3) sand. In this horizon the bleaching increases downslope and there is a higher proportion of coarse elements (centimetre-sized angular quartz fragments, ferruginous nodules). The presence of nodules is an extension from the already mentioned nodules in horizon (4), (7) and (8). At the upslope part of horizon (12), the coarse elements are separated from each other by a sandy clay matrix whereas downslope they are more frequently in contact with each

other. Towards the stream, horizon (12) becomes thicker and its organisation intersects the black soil system comprising of horizons (8) to (11). Horizon (12) is itself intersected by the incision of the talweg, but a similar sandy bleached material, although cemented probably by amorphous silica, was observed in the middle of the streambed.

A second bleached horizon (13) is observed within the saprolite of the gneiss between 11 and 1. It is about 0.8 meter thick close to the streambed, wedge-shaped and extends up to 30 m upslope.

Sequence T2 is located across a depression developed along a red soil-black soil contact (Fig. 10). The layout along T2 is almost similar to that along T1, except that it is not intersected by the incision of the streambed (Fig. 4e). In the depression, a sandy horizon, with location and characteristics similar to those of horizon (12) of T1, has developed at the top of the vertic clay horizon. At the downslope of horizon 12 although the texture is sandy, the vertic structure of a previously clay horizon is preserved (Fig. 4f) probably due to the cementation by amorphous silica. The shape and the size of the structure are similar in every respect to that observed in the clay vertic horizon (10).

4.8. Hydrodynamic behaviour of the red soil-black soil system

There is a strong contrast in the evolution of the water contents between A5 and A2 whereas along A3, A1 and A4 the evolution is intermediate. Therefore, the description here will be limited along these two end members, i.e., A5 for the red soil and A2 for the black soil. At the end of the dry season, a uniform 20% volumetric water content is found along the red soil profile A5 (Fig 11a, curve 1). At the beginning of the rainy season, the moisture content increases and the moisture front lowers regularly down to the saprolite (curve 2). During the wet season, the volumetric water content remains almost uniform along the profile, oscillating from about 30% immediately after the rainy events (curve 3) to 27% after draining the gravity water (curve 4).

Along A2, at the end of the 2004 dry season (Fig 11b, curve 1), the water content was more contrasted. Values of about 20% at 0.2 m depth increased progressively to about 27% in the vertic

clay horizon (9) and (10) between 0.8 to 1.8 m depth, and decreased again down to 20% in the saprolite (11) and, at further depth, reached 15 to 19% in the bleached horizon (13). Similar to what was described along the red soil profile, a regular progression of the moisture front is observed at the beginning of the wet season at the topsoil horizons (6) and (12) (curve 2 and 3). When the moisture front reached the clay horizon (8) and (9), the water rapidly descends to the bottom of the clay horizon (10) until the top of the saprolite (11) and the moisture content reaches 35% (curve 4). A strong rainfall event occurred on August 5, 2004 (Fig. 11c, curve 2). The water content increased by about 3 to 5% all along the profile whereas an abrupt increase was observed at 3 m in horizon (13). The water content increased up to 65% but this value is not reliable because it is beyond the calibration range of the neutron probe (maximum water content of 35%). A few hours later the water content had decreased again to about 20%, indicating that the water drained out quickly at horizon (13) (curve 3).

In 2005, the moisture conditions at the end of the dry season (Fig. 11c, curve 1) were very close to those at the same period in 2004 (Fig 11b, curve 1). The 2005 rainy season started earlier but with two main rainfall events in April and July separated by a dry period. In the black soil, a different behaviour of the moisture front was observed during these two rainy periods. During the first one, similar to what was observed during the previous rainy season of 2004, the moisture front reached clay horizon (8) and moved quickly along the profile A2 down to the top of the saprolite (11). During the dry interval, the moisture content decreased along the profile, and particularly in the topsoil horizon. At the following rainfall event, the moisture content increased again in the topsoil horizons with maximum water in the sandy horizon (12) (Fig 11c, curve 4). After a few days, the water content increased again in the clay horizons (8), (9) and (10).

5. Discussion

5.1. Reliability of the ECm survey

The experimental variogram built from EC_m data shows no nugget effect, which emphasizes that there is no variability in EC_m response at short distance. The absence of a nugget effect testifies to the stability of the EC_m values measured by the EM31 device. It also indicates that the high density of measurements is sufficient to take into account the variations and describe the spatial structure of conductivity at short distance. Moreover, the interspace between the transects (100 m) is below the range value of 300 m shown on figure 5, indicating that the density is also sufficient for a good assessment of EC_m distribution between the transects. The elaborated EC_m map is therefore a reliable tool for the extrapolation of soil and rock data on the studied area, and to discuss soil distribution.

5.2. Hydrological behaviour of an area vulnerable to erosion

The neutron probe monitoring carried out along sequence T1 shows two different types of hydrological behaviour of the black soil during the season.

At the beginning of the wet season, the cracks of the vertic clay horizon are open, favouring infiltration down to the saprolite after the moisture front reached the vertic horizons (9 and 10). This distinctive behaviour has often been described in black soils of South India (Hodnett and Bell, 1981). Several authors have observed that the cracks are usually open down to 2 m deep at the beginning of the wet season, and ending at the slickenside zone which is most strongly expressed at or just below the depth of the cracks in thick black soils (Kalbande et al., 1992). A similar information is given by Hodnett and Bell (1981), who found essentially no infiltration below the black soils where the clay horizons were deeper than 2 m whereas large quantities of water infiltrates at places where the saprolite is observed at less than 2 m deep and is reached by the cracks.

The effect of the swelling and closing of the cracks is emphasised with the neutron probe monitoring in 2005. During the first rainy event, the cracks are open and allow a fast distribution of the water down to the saprolite, whereas during the second one, the cracks are closed which significantly decreases the infiltration that results in the formation of a perched watertable in the subsurface at horizon 12. Radhakrishna and Vaidyanadhan (1994) reported that the seasonal changes in water infiltration in some black soils can shift from more than 70 $mm.h^{-1}$ at the beginning of the rainy season to less than 0.1 $mm.h^{-1}$ after swelling and closing of the cracks.

The monitoring along T1 also indicates a substantial but fleeting increase in the moisture content observed below 3 m depth during the floods (Fig 11c, curves 2 and 3). It is attributed to a lateral flow from the streambed into the porous horizon (13). The water is very quickly evacuated from horizon (13), which confirms that bleaching in this horizon can be attributed to a currently ongoing process.

5.3. Soil distribution and relative chronology in the soil cover

On the one hand, black soils mainly occur in the valley bottom although not exclusively, because they are also found at certain spots along the slope and at the crest line. On the other hand, black soils are sometime related to the presence of amphibolite, but they are not exclusively on amphibolites alone since they are frequently observed on gneiss saprolite as well. Therefore, although dry climate (< 1200 mm), downslope topography and lack of drainage are considered important factors in the development of black soils, our observations suggest that both topography and lithology have influenced their formation.

The soil cover morphology, comprising the layout of the horizons in cross section and more precisely the concordances or discordances between several sectors of the soil cover, make it possible to draw the relative chronology in the formation of the soil-streambed system. Five different ensembles are distinguished, namely the red soil, the black soil, the bleached horizon (12), the streambed, and the bleached horizon (13), and they are referred as systems A to E on Fig. 9b and 10.

The red soil system A is developed along the slopes under good drainage conditions, and consists of horizons concordant with the slope topography. The regular evolution from the saprolite of the gneiss to the topsoil suggests that this material is autochthonous and has developed from the gneiss. B is the black soil system with horizons concordant to the flat valley bottom and developed under bad drainage conditions. The following two arguments allow us to conclude that B progresses at the expense of A. 1. At the contact between the two systems A and B, we observed that B is developing from the base of the red soil system, first with the clay films on the structural faces of horizon (2), (3) and (4). The clay films are located around and not within the aggregates, and this pattern must be interpreted as formation and not destruction of clay material. 2. The morphology of the red soil is intersected by that of the black soil, indicating that the latter has developed more recently and at the expense of the red soil material. Within horizon (11), isolated volumes of the saprolite still preserve the orientation of the parental material, which indicate autochthony. The same is observed at the base of the black soil on the right side of the stream, and no morphological discontinuity nor evidence of alluvial/colluvial deposits has been detected towards the top of the black soil profile. Therefore, we suppose that the black soil has developed on autochthonous material. This point could be debated because the vertic horizon is known to homogenise the material due to the shrinkage-swelling effect, and could have removed a possible discontinuity in the soil profile. The structural approach alone does not make it possible to settle the argument.

On the left side of the stream, the morphology of the black soil B is in its turn intersected by the horizon (12) (C), which has therefore developed subsequently after B. Because C starts occurring close to the topsoil and just downslope from the contact between A and B, it suggests that C is induced by lateral and sub-surface drainage at the top of B where a perched watertable is fleetingly occurring during rainfall. It develops downslope due to a longer duration of the episaturation.

The fourth system (D) is the streambed itself, which intersects B and C. The black soil morphology B is horizontal and observed on both sides of the stream, and the vertic horizons (10) and (11) of the B system are in particular intersected by the streambed D. We conclude that the soil

cover, previously continuous and almost horizontal, was removed by the later incision of the streambed, which is also confirmed by the presence of roots crossing the streambed.

The streambed D also intersects unit C. The chronology of C with respect to the formation of the streambed is debatable. On the one hand, C could have been provoked or favoured by the drainage induced by the talweg and therefore have developed subsequently. One the other hand, C could have developed first and have been subsequently incised by the streambed. The soil cover morphology along sequence T2 shows that C is continuous and had developed before the incision of the streambed D (Fig. 4). Therefore, and because of the similarity in the morphology of both T1 and T2, it suggests that the same had occurred at T1.

Eventually, the bleached horizon (13) E has developed at the base of the black soil and within the saprolite of the gneiss. E intersects the red soil-black soil contact and is almost horizontal, i.e. concordant with the water level in the stream. Therefore we attribute the bleaching in E to the fast oscillation of the watertable induced by the stream and highlighted by the neutron probe monitoring. E is well developed on the left side of the stream in the gneiss saprolite, i.e. towards the red soil system. On the right side of the stream, however, the thickening of the vertic clay horizons (10) and (11) obstructs its development and it is therefore only a few decimetres wide.

5.4. Downslope landscape evolution

We previously concluded that the development of the streambed is a recent process that took place after the development of the soils. Moreover at the watershed scale, we observed that the streambed lies within the thin black soil, skirting around the thick black soil area. It suggests that the thin black soils have favoured or guided the development of the drainage network. Based on the above-mentioned observations of the relative chronology and hydrological behaviour of the soil cover we can propose a model of recent evolution for this downslope part of the landscape described in four steps (Fig. 12):

At stage 1, red soils occupy the slope, whereas black soils are developed on the flat valley bottom. At the beginning of the rainy season, the cracks are opened down to about 2 m deep in the thick black soil area and they end within the clay horizon, which prevents deep drainage. However, close to the border of the black soil area, although the cracks reach the same depth, they end at the sandy and permeable saprolite located below that enables the infiltration of a large quantity of water during the first events of the rainy season.

At stage 2, the chemical erosion or leaching is likely to have provoked the formation of a depression that will develop preferably in the thin black soils. Infiltration in the black soils occurs only at the onset of the wet season. During the rainy season and after the closing of the cracks, permeability of the black soils decreases and the depression behaves as a gutter collecting the runoff water. In its turn, the flow of water in the depression at the outer part of the black soil will favour the soil bleaching and horizons will progressively turn sandy.

Soil bleaching leads to stage 3 that corresponds roughly to the morphology observed along sequence T2. Observations at sequence T2 confirm that the formation of the streambed is preceded by the presence of the depression along the contact between red soil and black soil where the bleached system C has developed. The central part of the system C is cemented and a vertic structure is observed. The vertic structure could not have developed within the sandy material observed at present in system C but within a swelling clay horizon of the system B. During bleaching and textural change from B to C, the vertic structure is supposed to disappear. The presence of the vertic structure in C suggests that cementation and bleaching have occurred simultaneously, which made it possible to maintain the vertic structure in the sandy material C. On the left and at the contact between A and B the soil solution slows down, favouring the formation of clay coating around aggregates through over saturation of the soil solution with respect to silicate clays that led to the development of horizons (7), (8) and (9).

At stage 4, the streambed had developed down to the saprolite of the gneiss into the depression and in the sandy horizons of system C. A portion of C is preserved because of cementation by

amorphous silica. The presence of the streambed could favour the bleaching in horizon (12) at the top of the vertic clay. During the rainy season, the rapid oscillations of the watertable provoke the bleaching in the saprolite and the formation of system E.

5.5. Soil erosion relationships

The afore-described model for the formation of the soil cover is in agreement with the observations made at several scales on our study site. At the watershed scale, the model explains why the streambed is passing through the thin black soil area instead of crossing directly through the middle of the flat bottom area covered with thick black soil. At the scale of the sequence, the model is in agreement with the soil morphology observed along T2 and T1, respectively before and after the incision of the streambed. It also agrees with the hydrological behaviour in the black soil along soil profile A2. The development of the natural erosion in this area can be explained through the interaction of the stream and its distribution, with the type of soil cover and its hydrological behaviour. We will consider landform types 1, 2, and 3 successively.

Rotational slips (type 1) and seepage erosion (type 2) occur close to the contact between red and black soil. The type 1 features are favoured by the presence of system E. The neutron probe monitoring shows that a temporary watertable occurred very fleetingly within E when the water level was up in the stream. The thickening of the vertic clay horizon is obstructing the development of the system E towards the centre of the black soil area, but it developed predominantly from the streambed towards system A into the permeable saprolite. Because the system E is the plane of weakness for the erosion type 1, the rotational slips are also predominantly developed towards the red soil system A, and concern the whole soil cover down to the saprolite.

Seepage erosion (type 2) develops in system C at the upper part of the black soil. Because of the swelling in the black soil, the cracks get closed usually in the middle of the wet season, i.e. during the month of July. Later, heavy rainfall and less infiltration provoke the formation of a perched

watertable within C and the water flows sub-superficially towards the streambed. Whatever the process of clay elimination may be (leaching, ferrolysis…), the bleaching increases downslope resulting in a relative accumulation of the coarse elements, which become contiguous. Hence the whole bleaching process increases the vulnerability to erosion, which probably occurs in soaked (C) material during heavy rainfall, leading to sub-surface seepage erosion at the contact between (B) and (C).

The third type of erosion is not related to the red soil-black soil system, but to the non-cohesive sandy saprolite of the gneiss when it is exposed close to the topsoil. The erosion is due to the seasonal throughflow seepage of the watertable occurring within the sandy saprolite over the less permeable fractured rock during the rainy season. The combination between earthflow and sliding (type 3) occurs mostly in midslope positions (Fig. 8) and further studies should focus on it as a possible regional feature. In this case, these large erosional scars could influence the geomorphologic landscape evolution at wider scale and further study should also focus on the agreement between midslope erosion and the regional geomorphologic model proposed by Bourgeon and Gunnell (1998) and Gunnell et al. (2003).

6. Future directions

The objective of this study was to understand the distribution, dynamics and the factors intrinsic to the soil cover that are likely to influence or even govern the development of present and recent natural erosion in the forested area of South India. This aim was tackled through a structural approach of the soil cover, which includes the overlay of various types of survey at the watershed scale (electromagnetic induction, soil, geology, vegetation), and the study of concordances-discordances between horizons along representative soil sequences.

The present erosion is not randomly distributed. Three different types of erosion have been identified: Downslope rotational slips are governed by a temporary watertable within a bleached saprolite at the base of black soil-red soil transition. Seepage erosion is caused by a perched watertable occurring after closing of the cracks at the top of the vertic clay horizon of black soil. At midslope, a combination of earthflow and sliding occurred at places where the non-cohesive sandy saprolite of gneiss is exposed close to the topsoil.

Our study highlights the relative chronology in the development of the downslope soil cover and in particular we show that the geomorphology of valley bottoms and their erosion have been recently reactivated with the development of streambeds. Further research effort should focus on the study of the pedological processes prior or subsequent to the development of the streambeds in order to identify their contribution to the quality of the stream water. In particular, because silica cemented horizons have been observed at several points along the streambed, they are likely to be integral components of the soil system. Therefore, further study should focus on the identification of the soil forming processes that provide aqueous silica to this part of the system.

Acknowledgments

This study was supported through the research project “Kabini river basin” of ORE-BVET (Observatoire de Recherche en Environnement-Bassin Versant Expérimentaux Tropicaux, www.orebvet.fr), the French national programs “ECCO-PNRH” and “ACI-Eau” funded by IRD/INSU/CNRS, the Indo-French Centre for the Promotion of Advanced Research (IFCPAR WA-3000), and the Embassy of France in India. We thank Dr C. Camerlynck from UMR 7619 Sisyphe, University of Paris 6 for providing the EM31 equipment, Dr R. Wins (BRGM) for its contribution to the geological survey, the Karnataka Forest Department for providing the access to the site, and Dr. Vasanthi Dass for editorial advice.

References

Agarwala, V.P., 1985. Forests in India, Environmental and production frontiers. IBH Publications, New Delhi and Oxford, pp. 1-344.

Barbiéro, L., Mohamedou, A.Ould, Caruba, R., 1998. Influence de la maturation des sols de mangrove sur la déflation éolienne et la formation de dunes argileuses dans le delta du fleuve Sénégal. Comptes Rendus de l'Académie des Sciences Paris 327, 115-120.

Boulet, R., Bocquier, G., Millot, G. 1977. Géochimie de la surface et formes du relief. I., Déséquilibre pédobioclimatique dans les couvertures pédologiques de l'Afrique tropicale de Ouest et son rôle dans l'aplanissement des reliefs. Sciences Géologiques 30, 235-243.

Boulet, R., Chauvel, A., Humbel, F.X., Lucas, Y., 1982. Analyse structurale et cartographie en pédologie. I - Les études de toposéquences et principaux apports à la connaissance des sols. II - Une méthode d'analyse prenant en compte l'analyse tridimensionnelle des couvertures pédologiques. III - Passage de la phase analytique à une cartographie générale synthétique. Cahier ORSTOM, Série Pédologie 19, 309-351.

Bourgeon, G., 1991. Les "sols rouges" de l'Inde péninsulaire méridionale : Pédogenèse fersiallitique sur socle cristallin en milieu tropical. Doctorat Thesis, Université Paris VI, France.

Bourgeon, G., Pedro, G., 1992. Rôle majeur du drainage climatique dans la differentiation altéritique et pédologique des sols des regions chaudes. Comptes Rendus de l'Académie des Sciences Paris 314, 717-725.

Bourgeon, G., Gunnell, Y., 1998. Rôle du regime tectonique et du taux de denudation sur la repartition géographique et les propriétés des sols tropicaux. Comptes Rendus Académie des Sciences Paris 326, 167-172.

Braun, J.J., Ndam Ngoupayou, J.R., Viers, J., Dupré, B.,, Bedimo Bedimo, J.P., Boeglin, J.L., Robain, H., Nyeck B., Freydier, R., Sigha Nkamdjou, L., Rouiller, J., Muller J.P., 2005. Present weathering rates in a humid tropical watershed : Nsimi, South Cameroon. Geochimica et Cosmochimica Acta 69, 357-387.

Braun, J.J., Descloitres, M., Riotte, Barbiéro, L., Fleury, S., Boeglin, J.L., Ruiz, L., Sekhar, M., Mohan Kumar, M.S., Kumar, M.C., Dupré, B., 2006. Regolith thickness inferred from geophysical and geochemical studies in a tropical watershed developed on gneissic basement: Mulehole, Western Ghats (South India). Goldschmidt Conference Abstracts 2006, Geochimica et Cosmochimica Acta 70, Issue 18, Supplement 1, A65.

Bronger, A., Bruhn, N., 1989, Relict and recent features in tropical alfisols from South India, *in* Bronger, A., Catt, J.A. (eds.), Paleopedology. Catena Supplement 16, 107–128.

Bronger, A., Wichmann, P., Ensling, J., 2000. Over-estimation of efficiency of weathering in tropical "Red soil": its importance for geoecological problems. Catena 4, 181-197.

Brückner, H., Bruhn, N., 1992. Aspects of weathering and peneplanation in South India. Zeitschrift für Geomorphologie 91, 43-66.

Cannon, M.E., McKenzie, R.C., Lachapelle, G.P., 1994. Soil salinity mapping with electromagnetic induction and satellite based navigation methods. Canadian Journal of Soil Science 74, 335-343.

Corwin, D.L., Lesch, S.M., Oster, J.D., Kaffka, S.R., 2006. Monitoring management-induced spatio–temporal changes in soil quality through soil sampling directed by apparent electrical conductivity. Geoderma 131, 369-387.

Descloitres, M., Ruiz, L., Sekhar, M., Legchenko, A., Braun, J.J., Mohan Kumar, M.S., Subramanian, S., 2007, in press. Characterization of seasonal local recharge using Electrical Resistivity Tomography and Magnetic Resonance Sounding. Hydrological processes.

Dowd, P.A., 1982. Lognormal kriging - the general case. Mathematical Geology 14, 475-499.

Durand, N., Gunnell, Y, Curmi, P., Ahmad, S.M., 2006a, in press. Pathways of calcrete development on weathered silicate rocks in Tamil Nadu, India: Mineraly, chemistry and paleoenvironmental implications. Sedimentary Geology.

Durand, N., Gunnell, Y, Curmi, P., Ahmad, S.M., 2006b, in press. Pedogenic carbonates on Precambrian silicate rocks in south India. Orgin and paleoclimatic significance. Geological Society of America Special Paper.

FAO-ISRIC-ISSS, 1998. World reference base for soil resources. World soil resources report 84, FAO, Rome.

Filizola, H.F., Boulet, R., 1996. Evolution and opening of closed depressions developed in a quartz-kaolinitic sedimentary substratum at Taubaté basin (Sao Paulo, Brazil) and analogy to the slope evolution. Geomorphology 16, 77-86.

Fritsch, E., Peterschmitt, E., Herbillon, A.J., 1992. A structural approach to the regolith: Identification of structures, analysis of structural relationships and interpretations. Sciences Géologiques Bulletin 45, 77-97.

Furian, S., Barbiéro, L., Boulet, R., 1999. Organisation and dynamic of a soil mantel in tropical southeastern Brazil (Serra do Mar). Relation with landslides processes. Catena 38, 65-83.

Gaillardet, J., Dupré, B., Allègre, C.J., Négrel P., 1997. Chemical and physical denudation in the Amazon River Basin. Chemical Geology 142, 141-173.

Gaillardet, J., Dupré, B., Louvat, P., Allègre, C.J., 1999. Global silicate weathering and CO_2 consumption rates deduced from the chemistry of large rivers. Chemical Geology 159, 3-30.

Gunnell, Y., Bourgeon, G., 1997. Soils and climatic geomorphology on the Karnataka Plateau, peninsular India. Catena 29, 239-262.

Gunnell, Y., 2000. The characterization of steady state in earth surface systems: finding from the gradient modelling of an Indian climosequence. Geomorphology 35, 11-20.

Hodnett, M.G., Bell, J.P., 1981. Soil physical processes of groundwater recharge through Indian Black Cotton Soils. Institute of hydrology, Wellingford, UK, report 77, pp. 1-17.

Jacks, G., Sharma, V.P., 1995. Geochemistry of calcic horizons in relation to hillslope processes, Southern India. Geoderma 67, 203-215.

Kalbande, A.R., Pal, D.K., Deshpande, S.B., 1992. b-Fabric of some benchmark Vertisols of India in relation to their mineralogy. Journal of Soil Science 43, 375-385.

McNeill, J.D., 1980. Electromagnetic terrain conductivity measurement at low induction numbers. Technical Note TN-6, Geonics Ltd, Ontario, Canada.

Moyen, J.F., Martin, H., Jayananda, M., 2001. Multi- element geochemical modeling of crust-mantle interactions during late-Archean crustal growth: the Closepet Granite (South India). Precambrian Research 112, 87-105.

Murthy, R.S., Hirekerur, L.R., Deshpande, S.B., Venkat Rao, B.V., 1982. Benchmark Soils of India. National Bureau of Soil Survey and Land Use Planning, Nagpur, India.

Oliva, P., Viers, J., Dupré, B., 2003. Chemical weathering in granitic environments. Chemical Geology 202, 225-256.

Pal, D.K., Deshpande, S.B., 1987. Genesis of clay minerals in a red and black complex soils of southern India. Clay Research 6, 6-13.

Pascal, J.P., 1982. Forest map of South India, 1/250 000 scale, sheet Mercara-Mysore. Travaux Section Scientifique et Technique Institut Français de Pondichéry, hors série 18a.

Pascal, J.P., 1986. Explanatory booklet on the forest map of South India. Travaux Section Scientifique et Technique Institut Français de Pondichéry, hors série 18.

Planchon, O., Fritsch, E., Valentin, C., 1987. Rill development in a wet savannah environment. Catena Supplement 8, 55-70.

Radhakrishna, B.P., Vaidyanadhan, R., 1994. Black soils of Karnataka. In Radhakrishna, B.P., Vaidyanadhan, R., (Edts) Geology of Karnataka. Geological Society of India, Bangalore, 239-251.

Sidle, R.C., Pearce, A.J., O´Loughlin, C.L., 1985. Hillslope Stability and Land Use. Water Resources Monograph Series 11, American Geophysical Union, Washington D.C.

Singer, M. J. 1986. Bulk density-paraffin clod method. Pages 38-41. in: M.J. Singer and P. Janitzky (Editors). Field and Laboratory Procedures Used in a Soil Chronosequence Study. U.S. Geological Survey Bulletin 1648. U.S. Government Printing Office, Washington D. C.

White, A.T., Blum, A.E., Schulz, M.S., Vivit, D.V., Stonestrom, D.A., Larsen, M., Murphy, S.F., Eberl, D., 1998. Chemical weathering in a tropical watershed, Luquillo Mountains, Puerto Rico: I. Long term versus short term weathering fluxes. Geochimica Cosmochimica Acta 62, 209-226.

Figure captions

Table I: descriptive statistics of the erosion area at Mulehole watershed.

Fig. 1: Climatic gradient on the backslope of the Western Ghats (black lines are isohyets), main river course and location of the Mulehole studied site in southern India (modified from Gunnell and Bourgeon, 1997).

Fig. 2 : The studied watershed of Mulehole, topography (in metre), streams, North-South ECm measurement transects (…….) and soil sequences T1 and T2.

Fig. 3 : Plan view of the toposequence T1, red and black soils distribution, streambed and neutron probe access holes.

Fig. 4 : a) a rotational slip erosional landform (erosion type 1) was targeted for the excavation of a 80 m long trench (T1); b) seepage erosion (type 2) at the top of black soil profile; c) midslope erosional landform (type 3) resulting from the combination of seepage and mass movements into the non

cohesive material of the gneiss saprolite; d) rotational slip, the material has been partially evacuated; e) linear depression where the stream is currently incising; f) detail of the profile in the depression of T2 showing the vertic structure (defined by vertical and sub-horizontal cracks indicated by arrows) preserved in the sandy material due to silica cementation (knife is about 25 cm); g) roots of Tectona grandis crossing the streambed at about 1m high from the bottom, indicating recent incision.

Fig. 5 : Experimental variogram for electromagnetic conductivity (ECm) data and adjusted model.

Fig. 6 : Kriged map of soil electromagnetic conductivity (ECm) at the Mulehole watershed.

Fig. 7 : Lithological map of the studied area.

Fig. 8 : Soil cover on Mulehole watershed and distribution of erosion spots. 1- rotational slip; 2- seepage erosion at the top of black soil; 3- seepage erosion and mass movement in non-cohesive saprolite at midslope.

Fig. 9 : Cross section along the toposequence T1, showing a: the morphology of the red soil-black soil system (numbers refers to the horizons described in the text); b: Relationships with the development of the stream and the erosion type 1 and 2 (letters refers to the different steps in the development of the soil cover and streambed described in the text; cross-hatched area is part of (C) cemented by amorphous silica).

Fig. 10 : Morphology of the soil cover along the toposequence T2 showing the development of bleached horizon 12 in the depression before the incision by the stream (numbers refer to the horizons described in the text, and letters refer to the different steps in the development of the soil cover and streambed described in the text).

Fig. 11 : Neutron probe monitoring along red soil profile A5 (a), and black soil profile A2 (b) and (c), numbers on the curves refer to comments in the text.

Fig. 12 : Four-stage model showing the relative chronology in the recent formation of the soil cover at downslope. 1. Initial red soil-black soil contact (arrows denote the water flow along cracks and within the saprolite); 2. Development of the depression in the thin black soil; 3. Bleaching in the depression and hardening due to amorphous silica; 4. Incision of the stream and bleaching in the saprolite below the black soil (system E).

1

Erosion type	Number of spots	Mean eroded soil volume m^3	Standard deviation of eroded soil volume
Type 1: rotational slips	25	250	48
Type 2: seepage erosion	14	5	1.4
Type 3: recurrent combination of earthflow and sliding	7	3300	926

2

3 Table I: descriptive statistics of the erosion area at Mulehole watershed.

4

1 Fig. 1:

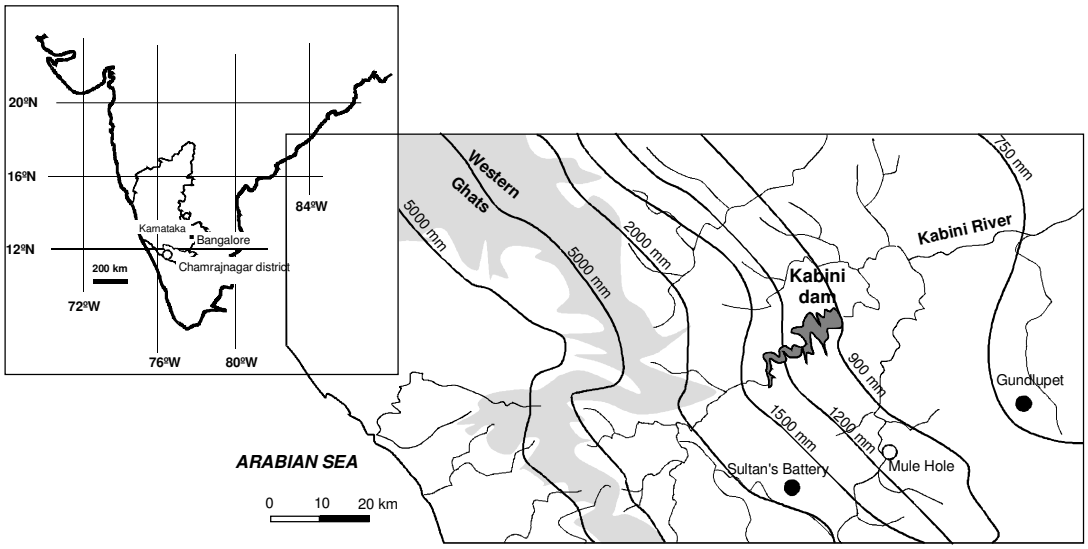
20ºN
16ºN
12ºN
72ºW
76ºW
80ºW
84ºW
Kamataka
Bangalore
Chamrajnagar district
200 km
Western Ghats
5000 mm
5000 mm
2000 mm
750 mm
Kabini River
Kabini dam
900 mm
1500 mm
1200 mm
Gundlupet
Mule Hole
Sultan's Battery
ARABIAN SEA
0 10 20 km

2

3

1 Fig. 2 :

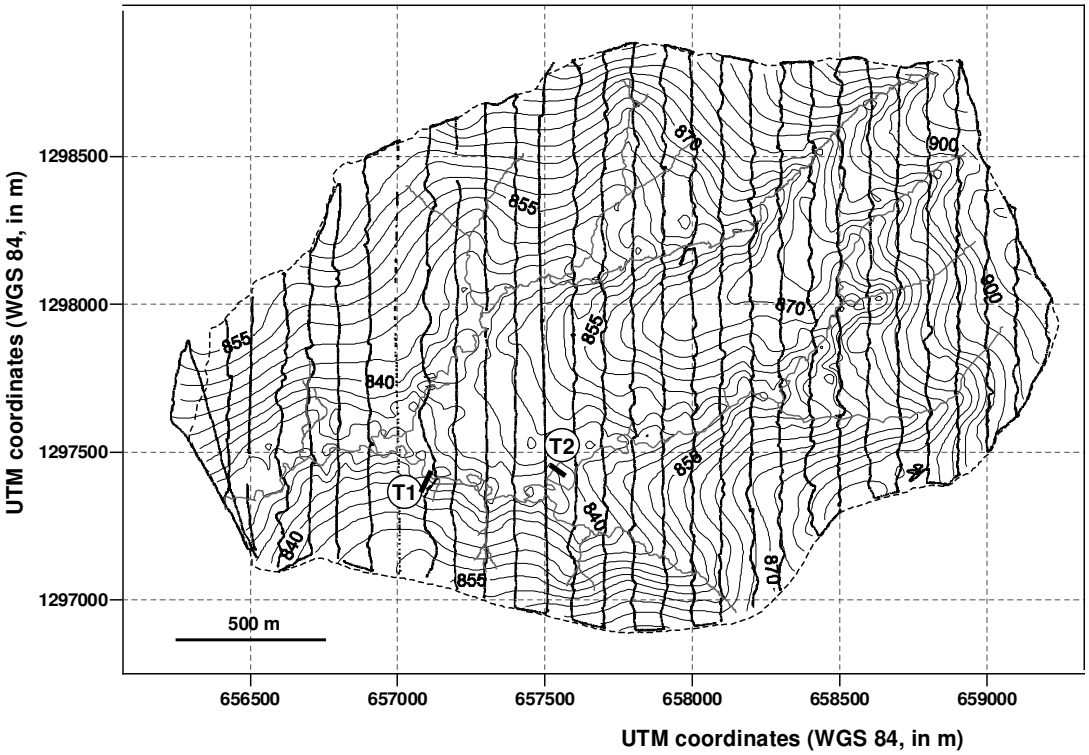
UTM coordinates (WGS 84, in m)
1298500
1298000
1297500
1297000
500 m
656500
657000
657500
658000
658500
659000
UTM coordinates (WGS 84, in m)
T1
T2
840
855
870
900

2
3
4

1 Fig. 3 :

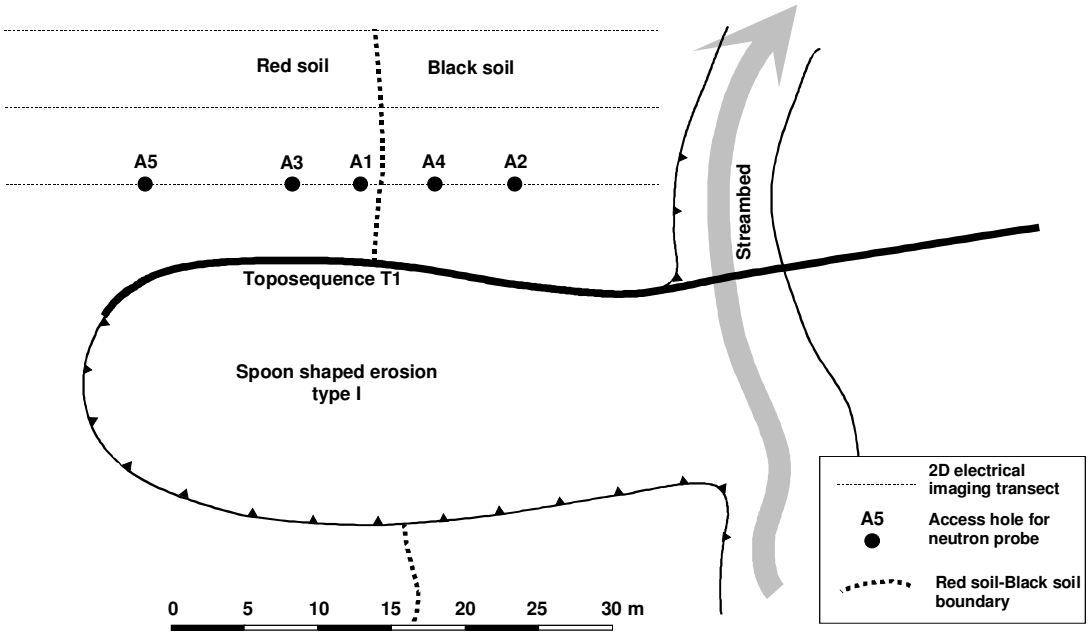
Red soil
Black soil
A5
A3
A1
A4
A2
Streambed
Toposequence T1
Spoon shaped erosion
type I
0
5
10
15
20
25
30 m
2D electrical
imaging transect
A5
Access hole for
neutron probe
Red soil-Black soil
boundary

2
3

a

b

c

d

e

Fig. 4:

f g

Fig. 4 (end):

1 Fig. 5 :

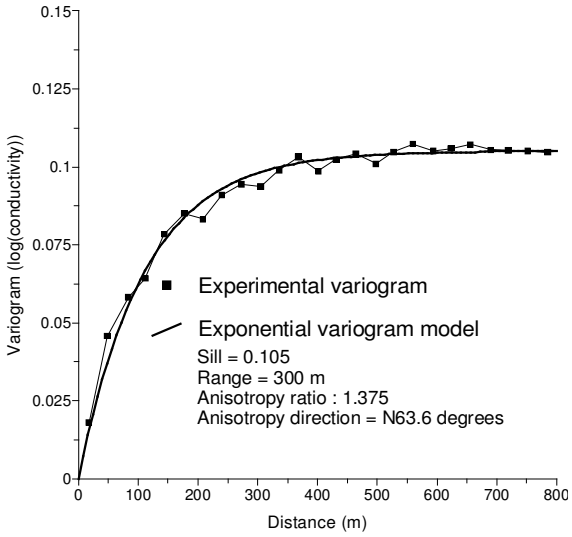
0.15
0.125
0.1
0.075
0.05
0.025
0
Variogram (log(conductivity))
0
100
200
300
400
500
600
700
800
Distance (m)
Experimental variogram
Exponential variogram model
Sill = 0.105
Range = 300 m
Anisotropy ratio : 1.375
Anisotropy direction = N63.6 degrees

2
3

1 Fig. 6 :

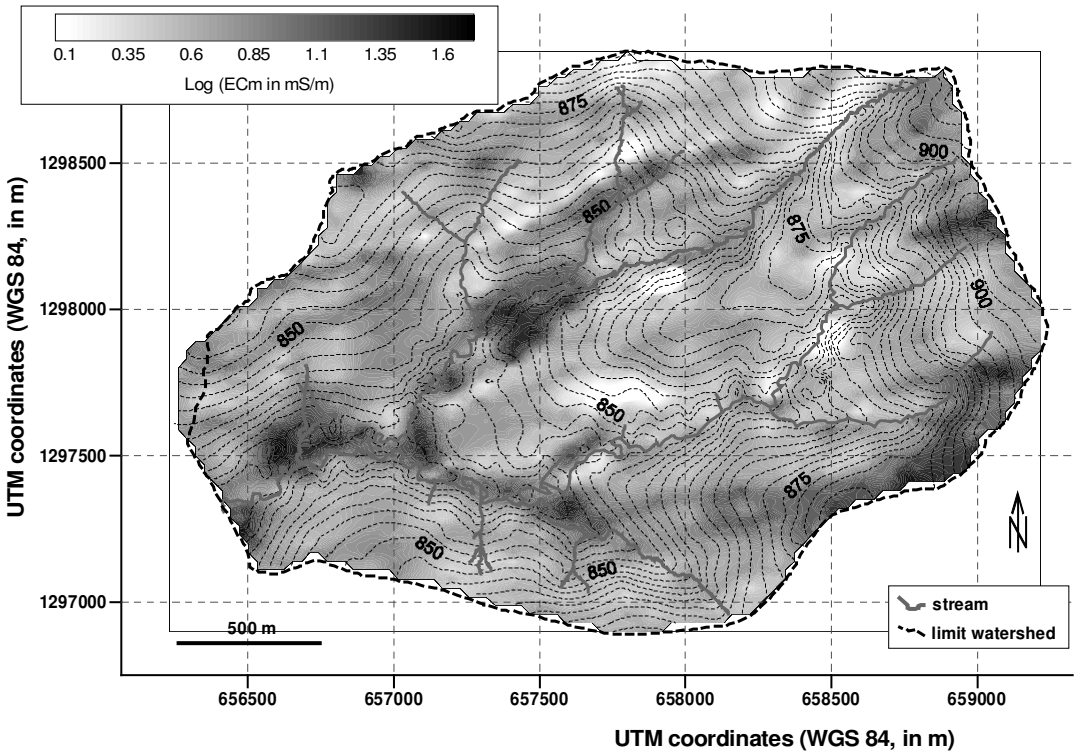
0.1 0.35 0.6 0.85 1.1 1.35 1.6
Log (ECm in mS/m)
875
900
850
875
900
850
850
875
850
850
1298500
1298000
1297500
1297000
500 m
stream
limit watershed
656500
657000
657500
658000
658500
659000
UTM coordinates (WGS 84, in m)
UTM coordinates (WGS 84, in m)

2
3

Fig. 7 :

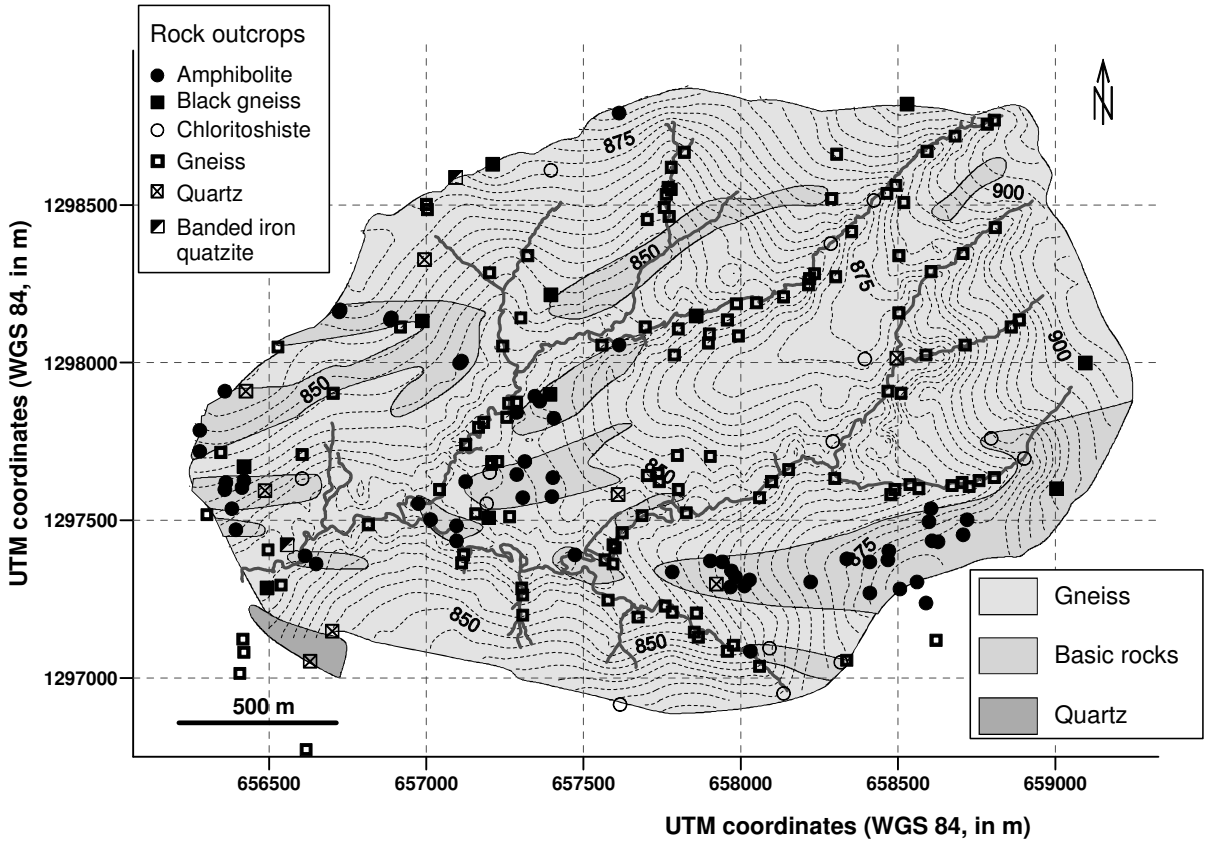
Rock outcrops
Amphibolite
Black gneiss
Chloritoshiste
Gneiss
Quartz
Banded iron quatzite
875
850
900
500 m
Gneiss
Basic rocks
Quartz
1298500
1298000
1297500
1297000
656500
657000
657500
658000
658500
659000
UTM coordinates (WGS 84, in m)
UTM coordinates (WGS 84, in m)

Fig. 8 :

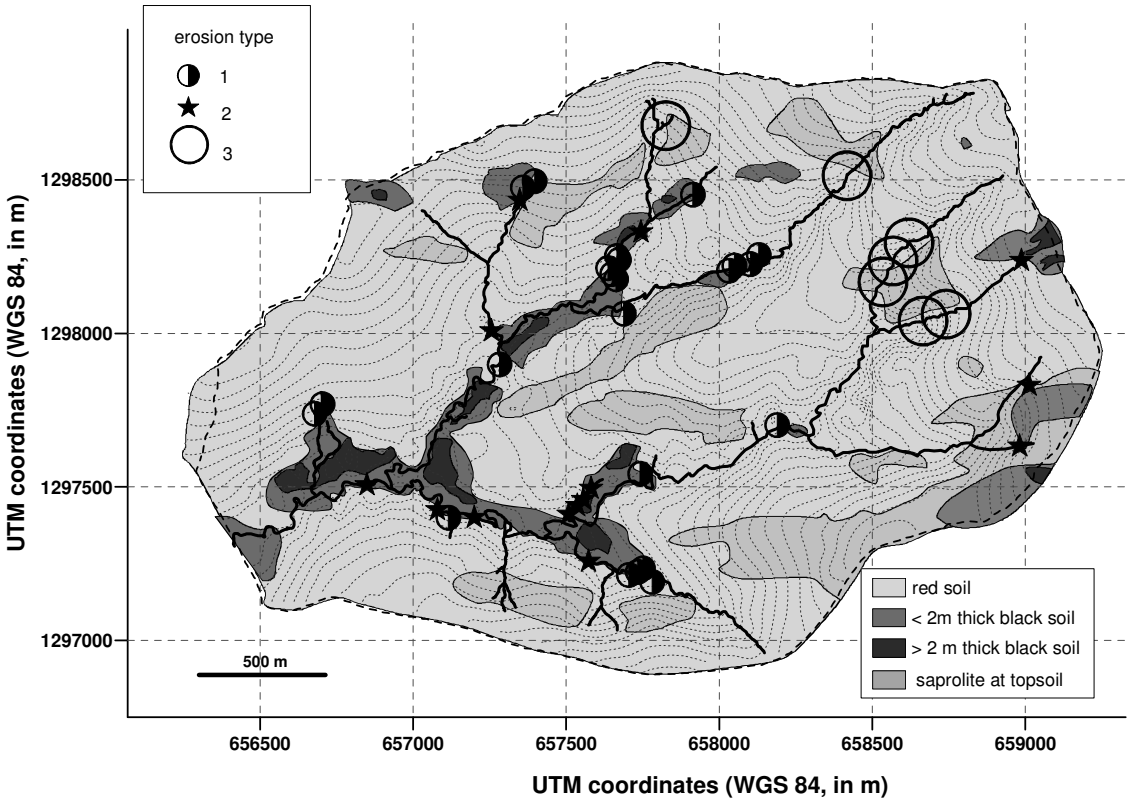
erosion type
1
2
3
1298500
1298000
1297500
1297000
UTM coordinates (WGS 84, in m)
500 m
red soil
< 2m thick black soil
> 2 m thick black soil
saprolite at topsoil
656500
657000
657500
658000
658500
659000
UTM coordinates (WGS 84, in m)

1 Fig. 9 :

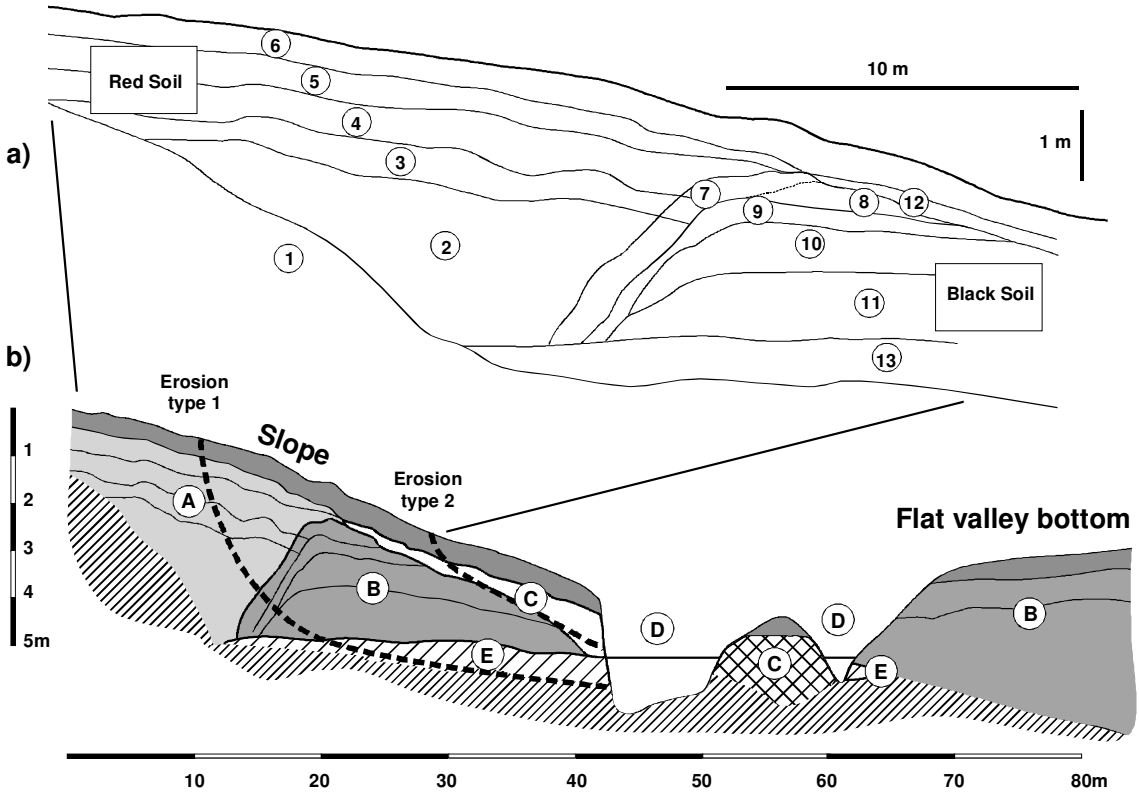
a)
Red Soil
Black Soil
10 m
1 m
1
2
3
4
5
6
7
8
9
10
11
12
13
b)
Erosion type 1
Slope
Erosion type 2
Flat valley bottom
A
B
C
D
E
1
2
3
4
5m
10
20
30
40
50
60
70
80m

2
3
4

1 Fig. 10 :

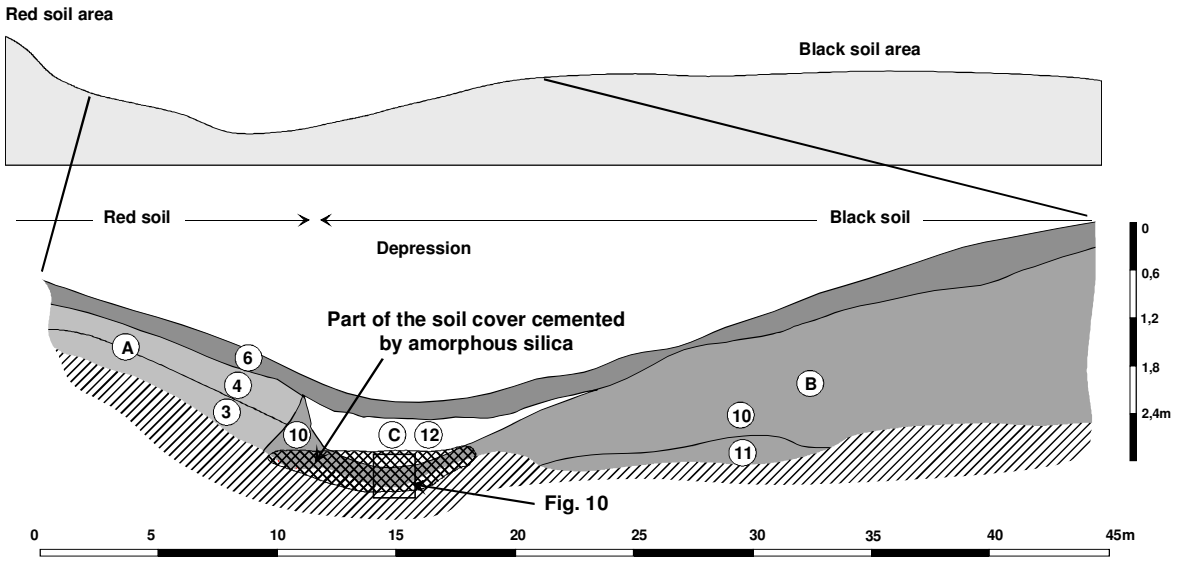
Red soil area
Black soil area
Red soil
Black soil
Depression
Part of the soil cover cemented by amorphous silica
A
6
4
3
10
C
12
B
10
11
Fig. 10
0
0,6
1,2
1,8
2,4m
0
5
10
15
20
25
30
35
40
45m

2
3
4

Fig. 11 :

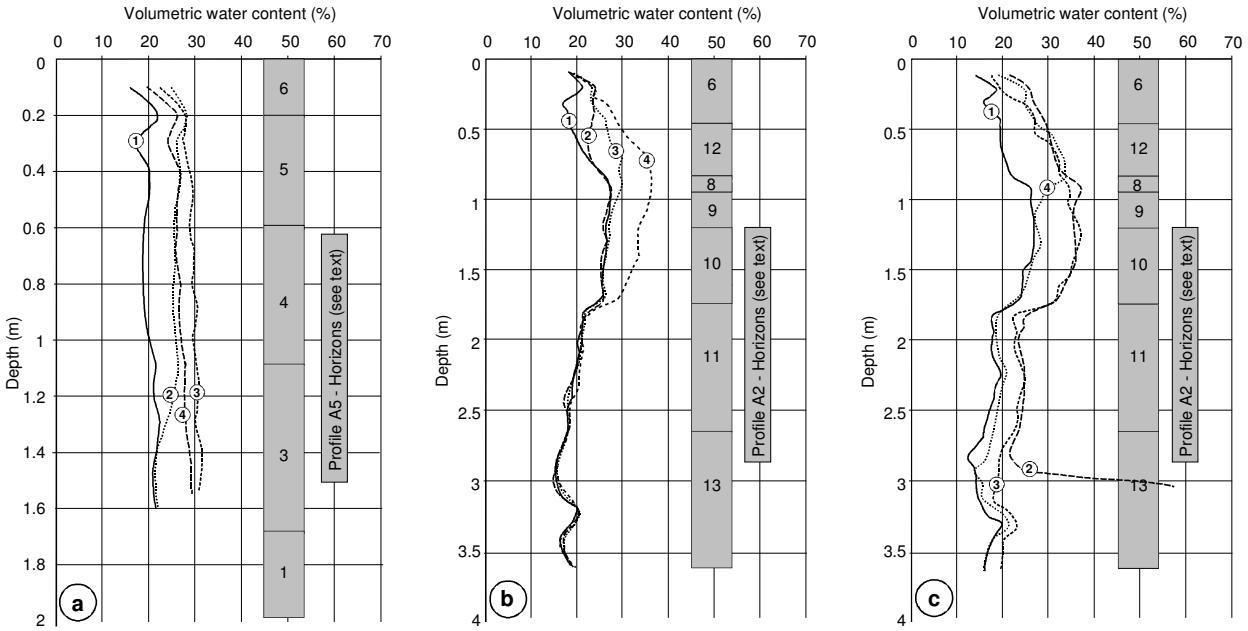
Volumetric water content (%)
Depth (m)
Profile A5 - Horizons (see text)
Profile A2 - Horizons (see text)
a
b
c

1 Fig. 12 :
2
3

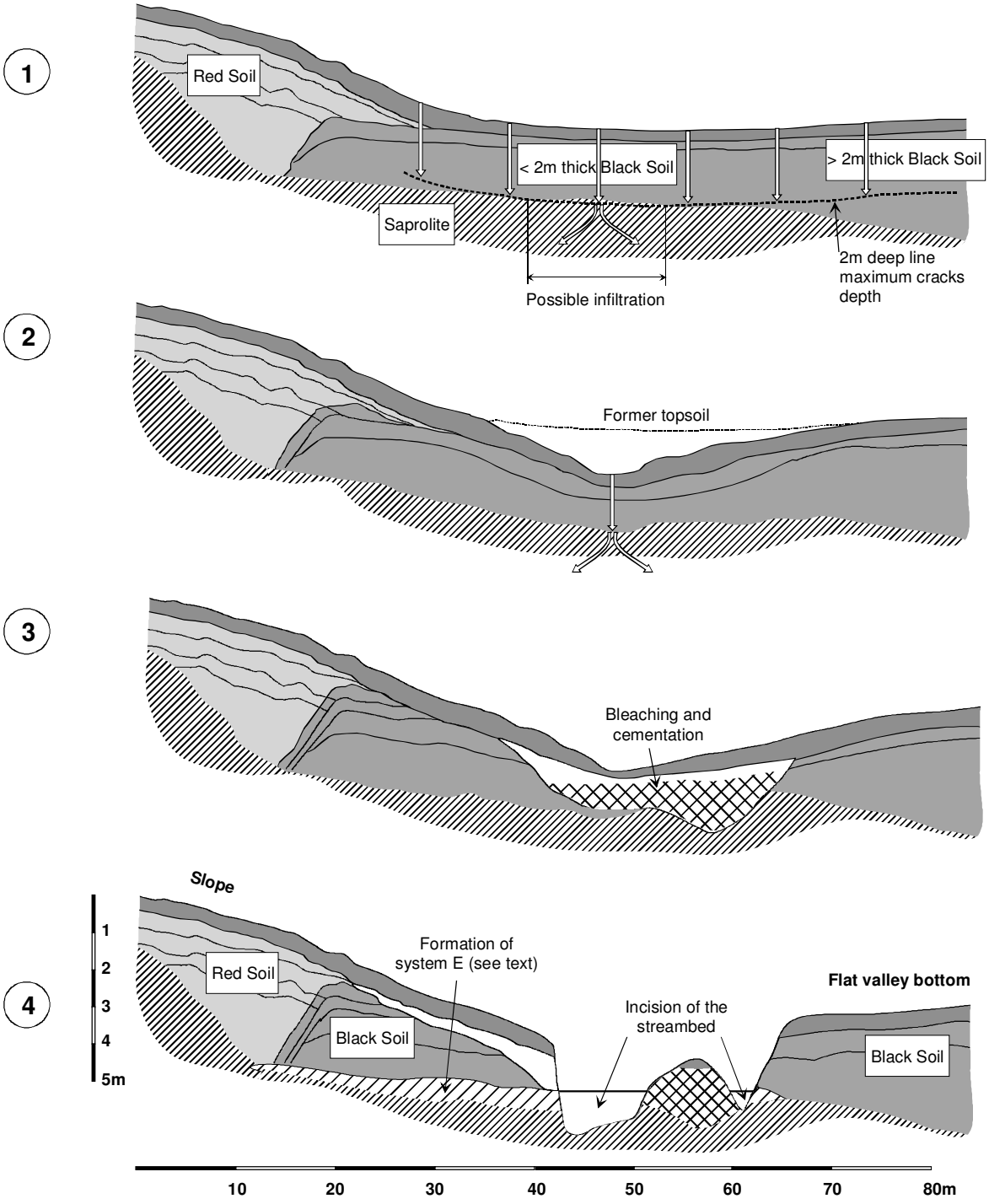
1
Red Soil
< 2m thick Black Soil
> 2m thick Black Soil
Saprolite
2m deep line
maximum cracks
depth
Possible infiltration
2
Former topsoil
3
Bleaching and
cementation
4
Slope
1
2
3
4
5m
Red Soil
Formation of
system E (see text)
Flat valley bottom
Incision of the
streambed
Black Soil
Black Soil
10
20
30
40
50
60
70
80m